Journal of Applied Physics ARTICLE scitation.org/journal/jap

Tunnel junction $I(V)$ characteristics: Review and a new model for p-n homojunctions

Cite as: J. Appl. Phys. **126**, 033105 (2019); doi: 10.1063/1.5104314
Submitted: 26 April 2019 · Accepted: 25 June 2019 ·
Published Online: 18 July 2019

N. Moulin, M. Amara,[a] F. Mandorlo,[b] and M. Lemiti[c]

AFFILIATIONS

University of Lyon, Lyon Institute of Nanotechnology (INL) UMR CNRS 5270, INSA de Lyon, Villeurbanne F-69621, France

[a]**Electronic mail:** mohamed.amara@insa-lyon.fr
[b]**Electronic mail:** fabien.mandorlo@insa-lyon.fr
[c]**Electronic mail:** mustapha.lemiti@insa-lyon.fr

ABSTRACT

Despite the widespread use of tunnel junctions in high-efficiency devices (e.g., multijunction solar cells, tunnel field effect transistors, and resonant tunneling diodes), simulating their behavior still remains a challenge. This paper presents a new model to complete that of Karlovsky and simulate an $I(V)$ characteristic of an Esaki tunnel junction. A review of different analytical models of band-to-band tunneling models is first presented. As a complement to previous work on tunnel junction simulation, the transmission coefficient is precisely determined and incorporated, the valley current between the tunneling and drift regimes is included, and calculations of physical parameters are updated. It is found that the model works for a broad range of values of the forward bias.

NOMENCLATURE

BGN	Band gap narrowing
$BTBT$	Band-to-band tunneling
c	Speed of light in vacuum
D_v	Volume density of occupied levels above E_V
E	Energy of an electron
E_C	Energy of the conduction band
E_{Fn}, E_{Fp}	Fermi levels on n and p sides
E_g	Bandgap
E_t	Carrier transverse energy
E_V	Energy of the valence band
F	Electric field
h	Planck constant
$\hbar$	Planck constant/2π
I_{BTBT}	Tunneling current
I_{Ch}	Excess tunnel current
I_P	Peak tunnel current
I_V	Valley current
k_B	Boltzmann constant
k_1	Wave vector of an electron of energy E
m_e	Effective mass of the electron
m_C, m_V	Effective mass of the electron on the conduction and valence bands
N_D, N_A	Density of donor and acceptor impurity atoms
n_i	Intrinsic carrier density
q	Charge of the electron
S	Junction surface
T	Temperature
TAT	Trap-assisted tunneling
TC	Transmission coefficient
TM	Transfer matrix method
V	Applied bias
V_{bi}	Built-in voltage
V_0	Barrier height
V_P	Voltage at $I = I_P$
V_V	Voltage at $I = I_V$
W	Free charge space
WKB	Wentzel–Kramers–Brillouin method
W_N, W_P	Depletion zone on n and p sides

Greek

θ	Parameter in Chynoweth's model

I. INTRODUCTION

The tunneling effect is a quantum phenomenon that allows carriers to cross a potential barrier without jumping over it. If the

barrier is thin enough and empty sites are available in the right range of energies, carriers from one side can tunnel to these empty sites. It should be noted that although the word "tunnel" carries the image of going through, it is rather the case that carriers disappear and then reappear on the other side of the barrier. The probability for this phenomenon to occur is highly correlated with the width of the barrier and the energy of the carrier. There are many devices (TFETs,[1] RTDs,[2] etc.) that rely on this effect for their properties, with specific materials and doping levels being chosen to create a tunnel effect. For example, in the field of photovoltaics, tandem solar cells score the highest efficiency on both laboratory and industrial scales by using tunnel junctions as key parts of their structures linking different subcells.[3]

However, there have been few studies focusing on the behavior of this particular component of these cells, and indeed, detailed simulations conducted by Hermle *et al.*[4] and Liu *et al.*[5] have highlighted the difficulty of such a task. A reliable tunneling model should be able to simulate three different regimes: the peak current, where tunneling is dominant; the valley current, where the tunneling probability is low and drifting starts to occur;[6,7] and the diode regime, where drifting is dominant. Yajima and Esaki discovered the tunneling effect experimentally in a highly doped germanium diode[8] in 1958, and Esaki[9] proposed a model to describe it. In 1960, an extensive theory was developed by Kane,[6] following a suggestion from Zener about a tunneling phenomenon. Soon after, Karlovsky[10] proposed a simpler version of the Esaki model that was valid as long as the difference between the gap and the Fermi levels was small enough. In 1969, the first review of tunneling models was presented by Duke.[11] In his book, he compared several models and approaches to establish which of these was the most accurate at that time. He considered, among others, the previous work by Kane and Esaki, as well as that by Keldysh,[12] who had found the same expression as Kane, although they had worked independently because of the lack of scientific communication between East and West during the Cold War.

As research on semiconductors progressed, several models were proposed (p–n diode, CMOS, SOI, III–V, etc.). In 1989, at a conference in Berlin, Hurkx *et al.*[13] presented a new model of the recombination rate based on the 1952 work of Shockley and Read[14] on Shockley–Read–Hall (SRH) recombination. This model was based on trap-assisted tunneling (TAT) associated with SRH recombination and band-to-band tunneling (BTBT) at reverse bias. In his paper, Hurkx calculated the contribution of the tunneling effect as a recombination rate instead of a current density. Along the same lines, in 1991, Klaassen[15] presented a model that was also mainly developed for TAT, since he considered this to be dominant over direct tunneling at forward-bias polarization.

Hurkx's work was tested in 2008 by Baudrit and Algora,[16] who underlined the fact that Hurkx's model does not work at forward bias. Currently, the reference model remains that of Tsu and Esaki.[17] Hermle *et al.*[4] presented a method to simulate an isolated GaAs tunnel junction at forward bias.

The first part of the present paper compares these analytical models in the context of simulation of direct BTBT. As far as the simulation method is concerned, a review of different analytical models and simulations leads to the conclusion that the nonlocal approach (see Fig. 1 of Ref. 5) is the most precise,[4,5,18] since it considers effective carrier transport. Also, only BTBT needs to be considered as the tunneling regime, since it is sufficient for correct simulation of an $I(V)$ curve.[4,5] The tunneling probability can be calculated using the transfer matrix method, since this method has proven to be accurate[5] and is computationally less expensive than the Wentzel–Kramers–Brillouin (WKB) method.[19] Simulations are run under Matlab software.

The main goal of this work is to construct an analytical model that is able to calculate $I(V)$ curves to aid in the design of the doping levels and dimensions of a tunnel diode. As the experimental work of the present authors is mainly concerned with silicon-based diodes, the review will focus on models that can be applied to this material.

II. REVIEW OF TUNNEL JUNCTION MODELS

A. Tsu–Esaki based models

1. Tsu–Esaki model

This model[17] is based on a previous one-dimensional (1D) superlattice model published in 1971.[20] The 1973 model incorporates a finite number of periods and a short electron mean free path. It also applies to multibarrier tunneling. The effective mass is calculated for unperturbed structures, and the 3D Schrödinger equation is solved for a 1D periodic potential V. Making the simplifying assumption that the transmission coefficient TC is a function of k_l only (the wave vector lies along the barrier dimension), we obtain

$$J = \frac{qm_e k_B T}{2\pi^2 \hbar^3} \int_0^\infty TC(E_l) \cdot \ln\left(\frac{1+\exp\left(\frac{E_{Fn}-E_l}{k_B T}\right)}{1+\exp\left(\frac{E_{Fp}-E_l-qV}{k_B T}\right)}\right) dE_l, \quad (1)$$

where m_e is the electron effective mass and E_l is the electron energy along k_l. This expression is general and holds regardless of the type of semiconductor (direct or indirect bandgap).

2. Kane model

In 1961, Kane developed a model[21] similar to Esaki and the later Karlovsky models, but using a different approach. This theory was adapted from Keldysh's[12] theory of indirect tunneling supplied by phonons. No transmission coefficient is calculated, but instead, the model is based on a function of the effective density of states, D_{Kane}, given by

$$D_{Kane} = \int [f_1(E_1) - f_2(E_2)] \left[1 - \exp\left(-\frac{E_1}{E_t}\right)\right] \times \left[1 - \exp\left(-\frac{E_2}{E_t}\right)\right] dE. \quad (2)$$

This function is zero when the electron has an energy outside the Fermi levels. Several subsequent models[15,22] have adopted similar functions. In Eq. (2), E_t is the transverse component of the electron energy, and subscripts 1 and 2 refer to the bands before and after tunneling. When a bias is applied, three regimes can be distinguished by comparing qV with the carrier energy. The tunneling current characteristic is thus mainly monitored by the function D_{Kane}, which takes into account the effect of phonons on the indirect tunneling process.

This model deals with the cases of direct and indirect semiconductors differently. As Si is of the latter type, we will focus on the corresponding model for our review.

3. Karlovsky model

Karlovsky[10] proposed a simple expression for the tunnel current in an Esaki diode based on the Esaki model,

$$E_1 = E_{Fn} - E_C, \quad E_2 = E_V - E_{Fp},$$
$$J = \frac{A}{S}\int_{E_C}^{E_V} \frac{E_{Fn} - E_{Fp}}{4k_B T}\sqrt{(E - E_C)(E_V - E)}dE, \tag{3}$$

where S is the surface area of the junction. This expression is valid if the distances between the Fermi levels and the edge bands (E_1 and E_2) are small ($\leq 2k_B T$). With $E_{Fn} - E_{Fp} = qV$, this expression becomes

$$J = \frac{A}{S}\cdot qV(E_1 + E_2 - qV)^2, \tag{4}$$

which is a polynomial function depending on the bias and the Fermi levels only. However, an uncertainty remains about the expression for A, which is not given explicitly in the original paper. By comparison with other models, it can be considered as a scaling factor.

4. Duke model

In 1969, Duke[11] presented what was then the state of art in tunneling theory, describing all the main tunneling models, their weak points, and their advantages.

The model simulated in this review is the one described as the most accurate at that period. In this model, the barrier profile is corrected by a coefficient introduced into the expression for the maximum electric field. However, it does not provide an accurate expression for the current when there is a high impurity concentration, and it tends to overestimate the valley current under a forward bias.

B. Recombination based models

1. Hurkx model

Hurkx[22] chose to calculate a recombination contribution rather than a tunnel current, using the following expression for BTBT,

$$R_{BTBT} = -B|F|^{\sigma} D_{Kane} \exp\left(\frac{-F}{F_0}\right), \tag{5}$$

where F is the local electric field. σ is a coefficient that is equal to 2 for direct tunneling and 2.5 for indirect tunneling (as in the case of silicon). D_{Kane} is calculated according to the theory of Keldysh[12] and Kane,[21] except that in the case of null and reverse bias, Hurkx proposes the following simpler expression:

$$D_{Hurkx} = \frac{1}{\exp\left(\frac{-E_{Fp} - qV}{k_B T}\right) + 1} - \frac{1}{\exp\left(\frac{-E_{Fn} - qV}{k_B T}\right) + 1}. \tag{6}$$

This function is equal to 1 when the electron energy is between E_{Fn} and E_{Fp} and 0 elsewhere.

This approach corresponds to what is known as the local tunneling model. Its drawbacks compared with the nonlocal approach in the case of tunneling theory were also pointed out by Hermle *et al.*[4]

2. Klaassen model

The Klaassen model is focused mainly on TAT. In the same way as in the Hurkx model, the tunneling contribution is calculated as a recombination factor R instead of a current density. The total tunneling effect is composed of two contributions: direct tunneling with R_{BTBT} given by Eq. (5) and a TAT mechanism at forward and reverse bias with

$$R = \frac{n_t p_t - r_n r_p n_i^2}{\tau_p(n_t + r_n n_l) + \tau_n(p_t + r_p n_l)} - R_{BTBT}, \tag{7}$$

where r_n and r_p are emission probabilities, n_t and p_t are the concentrations of tunneling carriers in the depletion region, and τ_n and τ_p are capture rates. The direct tunneling current density is then obtained by integrating the recombination factor,

$$R_{BTBT} = -\frac{dJ}{dE}\cdot F. \tag{8}$$

III. COMPARISON OF TUNNEL JUNCTION MODELS

A. Method and common parameters

The methods of calculation for material parameters (e.g., effective mass and intrinsic carrier concentration) and the ways in which physical phenomena (e.g., bandgap narrowing and the transmission coefficient) are taken into account differ among the models. Therefore, to allow a proper comparison, it is a necessary step to fix the calculation methods for both known and new physical parameters.

This work compares the models for a silicon p–n junction (without any oxide layer) at a high doping level.

One of the key parameters in a tunneling model is the transmission coefficient, which gives the probability for an electron at energy E to tunnel through a potential barrier of height V_0 and thickness a. The higher and thicker the barrier, the less probable it is that tunneling occurs. Accordingly, the higher the energy E, the more probable will tunneling be. Therefore, for a given height, there is a limiting thickness from which the probability starts to become negligible. Similarly, it is possible to determine a limiting energy from which electron tunneling is possible.

To calculate the tunneling probability, several methods have been developed, of which the two main ones are the Wentzel–Kramers–Brillouin (WKB) method and the transfer matrix method (TM). We have chosen to use the latter here, since it is more stable with respect to the geometry of the barrier and is computationally less expensive.[19] We use values of common physical parameters at 300 K as calculated by the most up-to-date methods (Table I).

B. Model comparison: Analysis

With the parameters listed in Table I, the current density curves are calculated for each model in forward bias (Fig. 1). What we expect is the typical "S" shape of a tunneling $I(V)$ curve.

TABLE I. Default parameters and references for their calculation.

Name	Value	Unit	Reference
T	300	K	
$N_C(300)$	2.89×10^{19}	cm^{-3}	Couderc *et al.*[23]
$N_V(300)$	1.04×10^{19}	cm^{-3}	Couderc *et al.*[23]
$n_{i0}(300)$	9.65×10^{19}	cm^{-3}	Couderc *et al.*[23]
E_A	45×10^{-3}	eV	Sze and Ng[24]
E_D	44×10^{-3}	eV	Sze and Ng[24]
BGN effect	ΔE_G	eV	Schenk[25]
Effective masses	m_c, m_v	kg	Couderc *et al.*[23]
N_A	8×10^{19}	cm^{-3}	
N_D	2×10^{20}	cm^{-3}	
S	64	μm^2	
V	[0, 0.5]	V	

- The Hurkx model works only for reverse bias[16] and, therefore, does not appear in the simulation for forward bias.
- The Tsu-Esaki and Duke models give a very low current density, and the results do not exhibit a tunneling peak at forward bias with these parameters, contrary to 1970 curves.[17]
- The Klaassen and Karlovsky models give an average current density, and the results exhibit a tunneling peak at forward bias. However, the Klaassen model does not apply after the peak, since the coefficient D_{Kane} is zero outside the tunneling regime [Eq. (2)].

In conclusion, this comparison reveals that the Karlovsky model gives the best shape for the tunneling $I(V)$ curve. However, it is incomplete and does not take into account important physical phenomena such as that represented by the transmission coefficient. Also, it does not cover the valley regime.

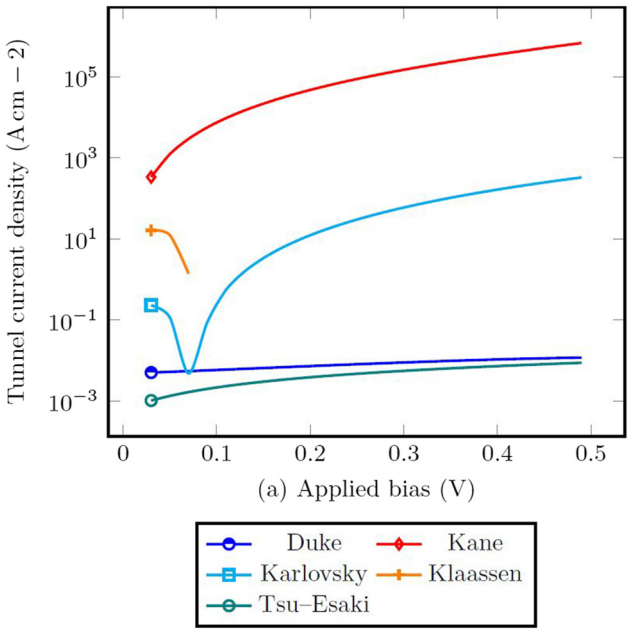

FIG. 1. Comparison of direct tunneling models at forward bias.

IV. NEW TUNNELING MODEL

A. General description

A new model to complete that of Karlovsky will be developed here by considering additional contributions from the tunneling current and the excess current. Each of these currents is linked to a specific type of carrier transfer. For the first, we consider a pure BTBT regime expressed by a third-degree polynomial P_3 weighted with a detailed TC. For the second, we consider a transition from a tunneling regime to a drift regime, using a TAT model developed by Chynoweth *et al.*:[7] I_{Ch}. This approach is similar to a semiempirical one developed by Demassa and Knott[26] and completed by Roy[27] in the early 1970s. Two scaling factors A and A' are introduced to balance the two contributions,

$$I = A.TC.P_3 + A' \cdot I_{Ch}. \tag{9}$$

B. Transmission coefficient

The simulation of a tunnel current is strongly linked with the transmission coefficient TC. This parameter gives the probability for an electron at a given energy to cross the junction. Among the various methods commonly used to calculate TC, we have chosen the TM method, since, as already mentioned, it is easy to implement and computationally less expensive.[19]

The standard TM method relies on two expressions,[28]

$$E < qV_0\text{: } TC = \frac{1}{1 + \frac{(qV_0)^2 \sinh^2(k_1 W)}{4E(qV_0 - E)}}, \tag{10}$$

$$E > qV_0\text{: } TC = \frac{1}{1 + \frac{(qV_0)^2 \sin^2(k_1 W)}{4E(E - qV_0)}}, \qquad k_1 = \sqrt{\frac{2m_e|qV_0 - E|}{\hbar^2}}. \tag{11}$$

Equation (10) calculates TC for electrons that can tunnel through a barrier of height V_0, whereas Eq. (11) calculates TC for electrons that can drift over the barrier (Fig. 2). The key task is to sort out those electrons that tunnel from those that drift over the barrier.

To understand how we incorporate TC into our model, it is necessary to understand what happens to the current between zero and the peak tunneling current $I_P(V_P)$, between I_P and the valley current $I_V(V_V)$, and after I_V [Fig. 3(a)]. When $0 < V < V_P$, the Fermi levels separate, and the occupied states come before the free states. With high doping levels, the barrier between the two sides of the junction is thin enough for tunneling to occur [Fig. 3(b)]. It should be noted that the BTBT regime is theoretically limited by E_{Fp} at the bottom and E_{Fn} at the top (in practice, a few carriers can be found above E_{Fn}, and BTBT is limited by E_V on the p side). In Fig. 2, the blue curve that shows the tunneling TC increases with the bias until it reaches a maximum (which corresponds to $V = V_P$).

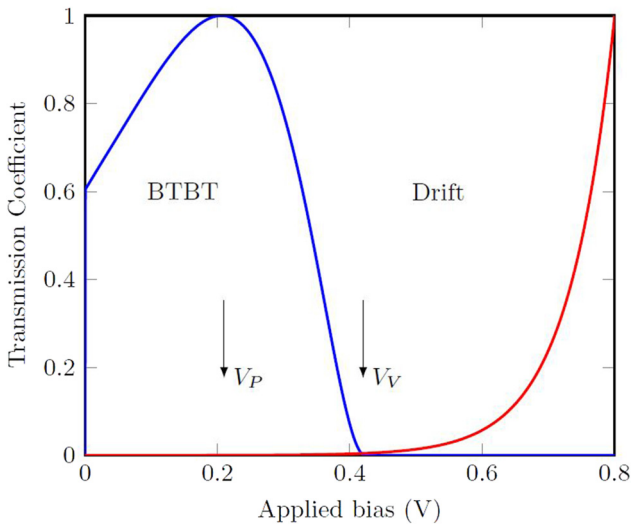

FIG. 2. Calculation of *TC* for tunneling (blue) and drift (red) regimes. The two curves have been normalized separately.

The red curve shows that almost no drift occurs at these values of bias.

When $V_P < V < V_V$, fewer and fewer states are located before the free states and can tunnel. Meanwhile, higher-energy states can no longer tunnel, and drifting starts to occur [Fig. 3(c)]. In Fig. 2, the tunneling *TC* decreases after V_P, and the drift *TC* starts to increase, revealing the transition from one regime to the other. At $V_V < V$, some occupied states are located above E_V and can no longer tunnel except by using traps located in the forbidden gap. However, more carriers with enough energy can drift over the barrier [Fig. 3(d)]. In Fig. 2, the blue curve is almost at zero, while the red curve begins to grow significantly.

Therefore, during the simulation, for each bias, we sort out two categories of electrons and apply the appropriate relation from Eq. (10) or (11). Following this, only the BTBT contribution to *TC* is retained and incorporated into the calculation of the current. As the drift probability is much higher than the tunneling probability, separating the two contributions allows better precision for the tunneling part of the $I(V)$ curve (Fig. 2, red and blue curves).

C. Tunneling regime

At low forward bias, two key values are considered: the peak current I_P, where the tunneling regime is at its highest, and the valley current I_V, where tunneling is at its lowest. In this model, the tunneling current is composed of two terms: *TC* and a third-degree polynomial P_3 inspired by the Karlovsky model,

$$I_{BTBT} = TC \cdot P_3, \tag{12}$$

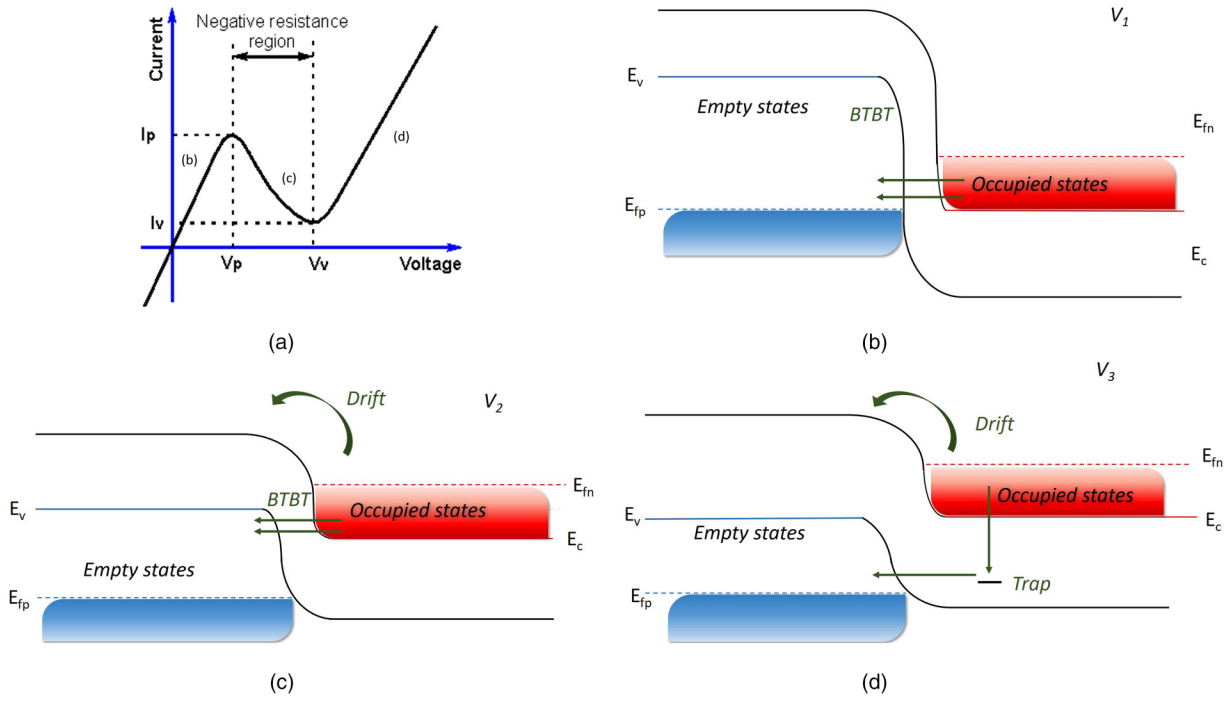

FIG. 3. Schematic representation of the evolution of a tunnel junction when a forward bias is applied. (a) Ideal tunnel diode $I(V)$ curve.[29] (b) Band diagram at low forward bias below V_P. (c) Band diagram at higher forward bias between V_P and V_V. (d) Band diagram at high forward bias above V_V.

$$\frac{\partial I_{BTBT}}{\partial V} = TC'(V) \cdot P_3(V) + TC(V) \cdot P_3'(V). \tag{13}$$

For there to be maxima at V_P and V_V, I_{BTBT} must satisfy the following conditions:

$$\text{At } V = 0\text{: } P_3(0) = 0, \tag{14}$$

$$\text{At } V = V_P\text{: } TC' = 0 \Rightarrow P_3'(V_P) = 0, \tag{15}$$

$$\text{At } V = V_V\text{: } TC \approx 0 \Rightarrow P_3(V_V) = 0. \tag{16}$$

In fact, the last condition is an approximation, since tunneling does not stop exactly at V_V but at a slightly higher bias. However, for this first approximation, it allows a local minimum at the correct position. These three conditions give us the expressions for the polynomial coefficients,

$$P_3 = V \cdot (V^2 - \nu_{pv} V + \nu_{pv} V_V - V_V^2), \tag{17}$$

with

$$\nu_{pv} = 3/2(V_V + V_P). \tag{18}$$

Modulo a scaling factor and TC, Eq. (17) gives the tunneling contribution to the $I(V)$ curve. We can see from the orange curve with the filled dot in Fig. 4 that the peak and valley tensions are aligned with the experimental data, but the slopes around I_P do not match exactly.

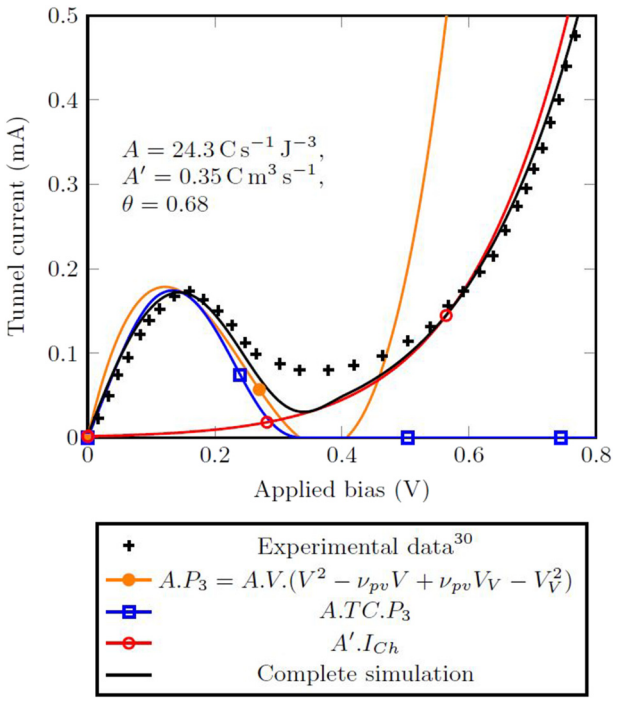

FIG. 4. Progressive improvements in simulation using Yan's[30] characteristic data for a silicon diode. $Na = 1 \times 10^{20}\,\mathrm{cm^{-3}}$, $Nd = 1 \times 10^{20}\,\mathrm{cm^{-3}}$, and $T = 300\,\mathrm{K}$.

D. Valley current

Because TC is calculated only for the BTBT regime, the last part of the polynomial curve is zero (Fig. 4, blue curve with a square). To simulate the drift regime, we choose to add another contribution based on an expression from Chynoweth *et al.*[7] that focuses mainly on the valley tunnel current,

$$I_{Ch} = D_v P, \tag{19}$$

with

$$P = \exp\left(-\frac{\alpha E_t^{3/2}}{F}\right), \tag{20}$$

$$E_t = E_G - qV + E_{Fn} + E_{Fp}, \tag{21}$$

$$F = 2\frac{\sqrt{V_{bi} - V}}{W}, \tag{22}$$

$$\alpha = \theta \cdot 4\frac{\sqrt{2m_e}}{3q\hbar} \quad \text{with } \theta \approx 1. \tag{23}$$

Here, E_t is the energy barrier faced by the carrier (which is equal to the difference between the two sides of the junction), F is the maximum field for a step junction, and P is the probability for a carrier to cross the gap (which is similar to what has previously been called TC). D_v is the volume density of occupied levels above the valence band for a given energy (i.e., the filled states in the defects for energies in the bandgaps). For a pure material, this density will be very low, thus resulting in a low excess current.

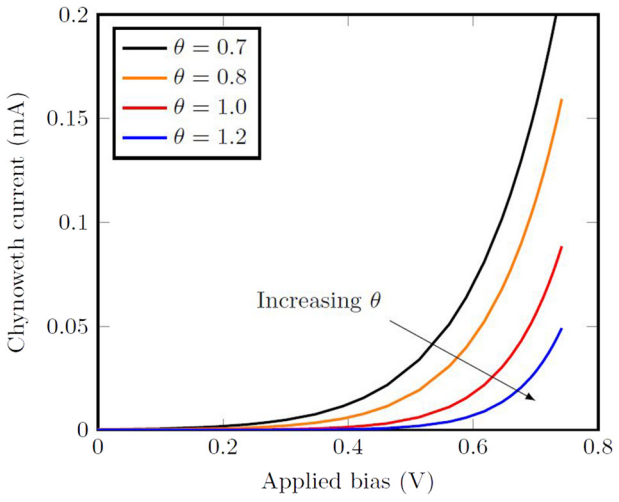

FIG. 5. Effect of θ on the shape of the valley current.

TABLE II. Contributions of the new model compared to previous most accurate model.

	Karlovsky model	New model
Tunneling peak	Yes	Yes
Valley fit	No	Partial
Voltage range	$[0, V_V]$	$[0, \gg V_V]$
TC	No	Yes
Drift fit	No	Yes
Bandgap narrowing	No	Yes

The expression for the tunnel current including this valley current is

$$I = A \cdot TC \cdot V(V^2 - \nu_{pv}V + \nu_{pv}V_V - V_V^2) + A' \cdot I_{Ch}(\theta). \quad (24)$$

The shape of the valley current depends mainly on θ (Fig. 5). Thus, the model has three input parameters (N_A, N_D, and the surface area S of the junction) and three fitting parameters (the scaling factors A, A', and θ). With this expression, the valley current is nonzero (Fig. 4, black full curve) and the drift part of the curve is consistent with experimental values. The remaining discontinuity at the valley current is a consequence of the initial hypothesis which approximates $TC(V_V)$ to 0 [Eq. (16)].

Table II lists the contributions of the new model compared to the Karlovsky model.

E. Effect of temperature

As mentioned for the Karlovsky model, the hypotheses leading to the third-degree polynomial are valid as long as the widths of the Fermi levels are smaller than $2k_BT$. An abscissa (Fig. 6) can be drawn to find the limiting doping level for each temperature. Below these limits, the hypotheses of the model are valid. Above them, the model can still be used, but with caution. For example, for junctions with high doping levels, the model is more accurate at high temperatures. The limits at $3k_BT$ and $4k_BT$ are quite far from $2k_BT$ (Fig. 6), so exceeding the limit by 10% does not strongly affect the accuracy of the model.

In Fig. 7, the experimental data and the doping levels are the same as those considered in Sec. IV C, and the parameters are calculated for temperatures ranging from 100 to 500 K. When the temperature increases, we can see that the positions of V_P and V_V do not vary. However, there is a small shift toward higher current at V_P and a greater shift in current at V_V. These shifts have been observed experimentally by Schmid *et al.*,[31] who found a significant vertical shift at V_V for junctions with a peak-to-valley current ratio (PVCR) of 2.63. For junctions with a PVCR of 1.5, there was a small shift at V_P and a vertical shift at V_V. The junction considered in the present paper has a PVCR of 2.17. Therefore, the shifts observed in the simulation are consistent with the experimental curves described by Schmid *et al.*[31]

Experimental data are supposed to be measured at room temperature. This is confirmed by the fact that the best fit is obtained for the simulation at 300 K (cyan dashed line).

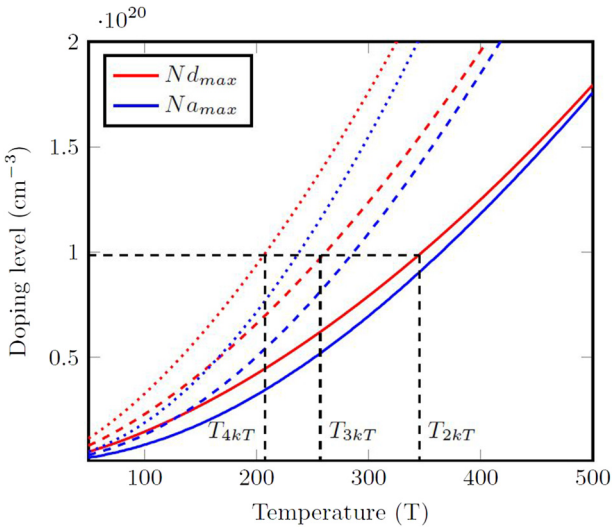

FIG. 6. Doping levels at which $E_C - E_{Fn}$ and $E_V - E_{Fp}$ are equal to $2k_BT$ (solid curve), $3k_BT$ (dashed curve), and $4k_BT$ (dotted curve) for silicon.

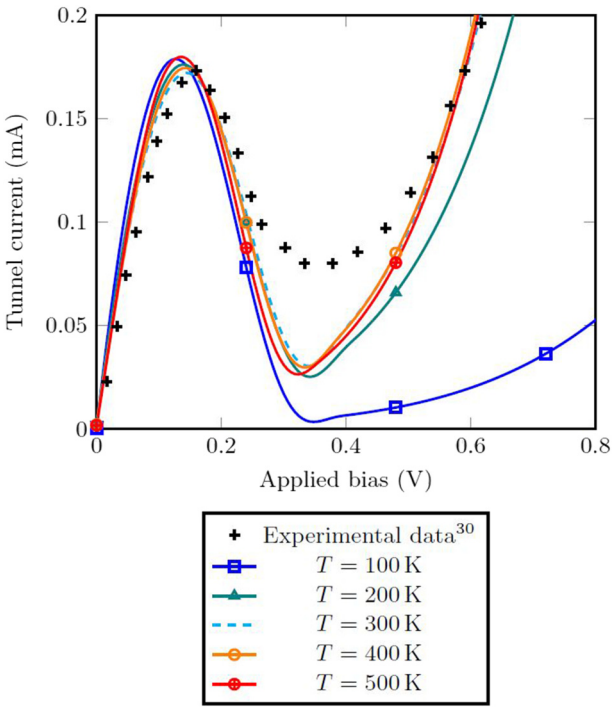

FIG. 7. Impact of temperature on a tunnel diode.

V. CONCLUSIONS

In this paper, different analytical models for a p–n tunnel junction have been investigated and compared. This review has revealed that recombination models have a limited range of validity and are not easy to implement. A new model to complete that of Karlovsky has been proposed, with the following new aspects:

- accurate calculation of physical parameters taking account of extra phenomena such as bandgap narrowing and degenerate Fermi levels;
- decomposition of the model into two contributions (tunneling and valley);
- incorporation of the transmission coefficient;
- incorporation of the valley regime using the model of Chynoweth *et al.*; and
- prediction of temperature effects that are consistent with experimental results.

This model, valid at high temperature, shows a good correlation with experimental data.

In this work, only BTBT has been considered, since it is assumed to be dominant in materials with low impurity concentrations. Also, from the work of Hermle *et al.*,[4] it appears that the inclusion of a TAT mechanism does not lead to any significant changes in the simulated curves. Also, a nonlocal approach as recommended by Hermle *et al.*[4] has been adopted by modeling carrier transport through a transmission coefficient.

Further investigations could include finding a detailed expression for the valley current and extending this model to heterojunctions. The latter should consider other tunneling effects than pure *BTBT* and incorporate them in the calculation of *TC*. Energy band offset at the interface between the two materials may induce additional modifications.

REFERENCES

[1]R. Abadi and M. Saremi, "A resonant tunneling nanowire field effect transistor with physical contractions: A negative differential resistance device for low power very large scale integration applications," J. Electron. Mater. **47**, 1091–1098 (2017).
[2]A. Goharrizi, M. Zoghi, and M. Saremi, "Armchair graphene nanoribbon resonant tunneling diodes using antidote and bn doping," IEEE Trans. Electron Devices **63**, 3761–3768 (2016).
[3]M. A. Green, "Intrinsic concentration, effective densities of states, and effective mass in silicon," J. Appl. Phys. **67**, 2944–2954 (1990).
[4]M. Hermle, G. Létay, S. P. Philipps, and A. W. Bett, "Numerical simulation of tunnel diodes for multijunction solar cells," Prog. Photovoltaics Res. Appl. **16**, 409–418 (2008).
[5]Y. Liu, M. Ahmadpour, J. Adam, J. Kjelstrup-Hansen, H.-G. Rubahn, and M. Madsen, "Modeling multijunction solar cells by nonlocal tunneling and subcell analysis," IEEE J. Photovoltaics **8**, 1363–1369 (2018).
[6]E. O. Kane, "Zener tunneling in semiconductors," J. Phys. Chem. Solids **12**, 181–188 (1960).
[7]A. G. Chynoweth, W. L. Feldmann, and R. A. Logan, "Excess tunnel current in silicon Esaki junctions," Phys. Rev. **121**, 684 (1961).
[8]L. Esaki, "New phenomenon in narrow germanium p-n junctions," Phys. Rev. **109**, 604–605 (1958).
[9]T. Yajima and L. Esaki, J. Phys. Soc. Jap. **11**(13), 1281–1287 (1958).
[10]J. Karlovsky, "Simple method for calculating the tunneling current of an Esaki diode," Phys. Rev. **127**, 419–419 (1962).
[11]C. Duke, *Tunneling in Solids*, Solid State Physics (Academic Press, New York, 1969).
[12]L. V. Keldysh, "Behaviour of non-metallic crystals in strong electric fields," Sov. Phys. JETP **6**, 763 (1958).
[13]G. A. M. Hurkx, F. G. O'Hara, and M. P. G. Knuvers, "Modelling forward-biased tunneling," in *Solid State Device Research Conference, 1989* (IEEE, 1989), pp. 793–796.
[14]W. Shockley and W. T. Read, Jr., "Statistics of the recombinations of holes and electrons," Phys. Rev. **87**, 835 (1952).
[15]*Simulation of Semiconductor Devices and Process*, edited by W. Fichtner and D. Aemmer (Zurich, Switzerland, 1991), Vol. 4.
[16]M. Baudrit and C. Algora, "Modeling of GaInP/GaAs dual-junction solar cells including tunnel junction," in *2008 33rd IEEE Photovoltaic Specialists Conference (PVSC'08)* (IEEE, 2008), pp. 1–5.
[17]R. Tsu and L. Esaki, "Tunneling in a finite superlattice," Appl. Phys. Lett. **22**, 562–564 (1973).
[18]M. Baudrit and C. Algora, "Tunnel diode modeling, including nonlocal trap-assisted tunneling: A focus on III-V multijunction solar cell simulation," IEEE Trans. Electron Devices **57**, 2564–2571 (2010).
[19]A. Gehring, "Simulation of tunneling in semiconductor devices," Ph.D. dissertation (Technischen Universität Wien, 1975).
[20]R. Tsu and L. Esaki, "Nonlinear optical response of conduction electrons in a superlattice," Appl. Phys. Lett. **19**, 246–248 (1971).
[21]E. O. Kane, "Theory of tunneling," J. Appl. Phys. **32**, 83–91 (1961).
[22]G. A. M. Hurkx, D. B. M. Klaassen, and M. P. G. Knuvers, "A new recombination model for device simulation including tunneling," IEEE Trans. Electron Devices **39**, 331–338 (1992).
[23]R. Couderc, M. Amara, and M. Lemiti, "Reassessment of the intrinsic carrier density temperature dependence in crystalline silicon," J. Appl. Phys. **115**, 115–119 (2014).
[24]S. M. Sze and K. K. Ng, *Physics of Semiconductor Devices* (John Wiley Sons, Inc., 2007).
[25]A. Schenk, "Finite-temperature full random-phase approximation model of band gap narrowing for silicon device simulation," J. Appl. Phys. **84**, 3684–3695 (1998).
[26]T. A. Demassa and D. P. Knott, "The prediction of tunnel diode voltage-current characteristics," Solid State Electron. **13**, 131–138 (1970).
[27]D. Roy, "On the prediction of tunnel diode I–V characteristics," Solid State Electron. **14**, 520–523 (1971).
[28]C. Cohen-Tannoudji, B. Diu, and F. Laloe, *Quantum Mechanics, 2 Volume Set* (Wiley, 1992).
[29]ECE Tutorials Electronics and Control System, see http://ecetutorials.com/analog-electronics/tunnel-diode/ for "Tunnel diode—Working principle and characteristics."
[30]Y. Yan, "Silicon-based tunnel diode technology," Ph.D. dissertation (University of Notre Dame, 2008).
[31]H. Schmid, C. Bessire, M. T. Björk, A. Schenk, and H. Riel, "Silicon nanowire Esaki diodes," Nano Lett. **12**, 699–703 (2012).